

Small Molecule-facilitated Degradation of ANO1 Protein

A NEW TARGETING APPROACH FOR ANTICANCER THERAPEUTICS

Received for publication, January 10, 2014, and in revised form, February 24, 2014. Published, JBC Papers in Press, March 5, 2014, DOI 10.1074/jbc.M114.549188

Anke Bill[‡], Michelle Lynn Hall^{‡1}, Jason Borawski[‡], Catherine Hodgson[§], Jeremy Jenkins[‡], Philippe Piechon[¶], Oana Popa[§], Christopher Rothwell[‡], Pamela Tranter[§], Scott Tria[‡], Trixie Wagner[¶], Lewis Whitehead[‡], and L. Alex Gaither^{‡2}

From the [‡]Novartis Institutes for Biomedical Research, Cambridge, Massachusetts 02139, the [§]Novartis Institutes for Biomedical Research, Horsham, West Sussex, RH12 5AB, United Kingdom, and the [¶]Novartis Institutes for Biomedical Research, Basel CH-4002, Switzerland

Background: The calcium-activated chloride channel ANO1 is highly expressed in cancer.

Results: Inhibition of ANO1 activity alone is not sufficient to inhibit cancer cell proliferation, suggesting a novel function of ANO1 protein in cancer.

Conclusion: The ANO1 inhibitor CaCC_{inh}-A01 inhibits cancer cell proliferation by facilitating degradation of ANO1.

Significance: Our results may provide a new targeting approach for antitumor therapy in ANO1-amplified cancers.

ANO1, a calcium-activated chloride channel, is highly expressed and amplified in human cancers and is a critical survival factor in these cancers. The ANO1 inhibitor CaCC_{inh}-A01 decreases proliferation of ANO1-amplified cell lines; however, the mechanism of action remains elusive. We explored the mechanism behind the inhibitory effect of CaCC_{inh}-A01 on cell proliferation using a combined experimental and *in silico* approach. We show that inhibition of ANO1 function is not sufficient to diminish proliferation of ANO1-dependent cancer cells. We report that CaCC_{inh}-A01 reduces ANO1 protein levels by facilitating endoplasmic reticulum-associated, proteasomal turnover of ANO1. Washout of CaCC_{inh}-A01 rescued ANO1 protein levels and resumed cell proliferation. Proliferation of newly derived CaCC_{inh}-A01-resistant cell pools was not affected by CaCC_{inh}-A01 as compared with the parental cells. Consistently, CaCC_{inh}-A01 failed to reduce ANO1 protein levels in these cells, whereas ANO1 currents were still inhibited by CaCC_{inh}-A01, indicating that CaCC_{inh}-A01 inhibits cell proliferation by reducing ANO1 protein levels. Furthermore, we employed *in silico* methods to elucidate novel biological functions of ANO1 inhibitors. Specifically, we derived a pharmacophore model to describe inhibitors capable of promoting ANO1 degradation and report new inhibitors of ANO1-dependent cell proliferation. In summary, our data demonstrate that inhibition of the channel activity of ANO1 is not sufficient to inhibit ANO1-dependent cell proliferation, indicating that the role of ANO1 in cancer only partially depends on its function as a channel. Our results provide an impetus for gaining a deeper understanding of ANO1 modulation in cells and introduce a new targeting approach for antitumor therapy in ANO1-amplified cancers.

Transformation of a normal cell to a cancer cell requires the acquisition of genetic abnormalities. Cancer cells become addicted to these driving factors, providing promising targets for therapeutic intervention (1). ANO1 has been shown to be amplified and highly expressed in several human carcinomas, including gastrointestinal stromal tumors, head and neck squamous carcinoma (HNSCC),³ esophageal squamous carcinoma (ESCC), and breast cancer (2–7). The coding sequence of ANO1 is located within the 11q13 amplicon, a genomic region that is frequently amplified in various human cancers, such as HNSCC, ESCC, gastrointestinal stromal tumors, and breast and bladder cancer. Overexpression and amplification of ANO1 in cancer had been described long before its molecular identity and function was discovered, resulting in multiple nomenclatures for ANO1 (also known as TMEM16A, DOG1, OROV2, and TAOS2). It is now well established that ANO1 is an eight-transmembrane protein and that ANO1 functions as a calcium-activated chloride channel (CaCC) localized at the plasma membrane (8–10). ANO1 is physiologically expressed in multiple tissues, including secretory epithelia, smooth muscles, and sensory neurons, and is involved in regulation of airway fluid secretion, gut motility, secretory functions of exocrine glands, vascular smooth muscle contraction, and nociception (8–12). Therefore, dysregulation of ANO1 plays a critical role in several disease states, including pulmonary diseases, hypertension, diarrhea, and cancer (2–7, 11, 13). Not surprisingly, knockout of ANO1 is embryonic lethal (14). Amplification of ANO1 correlates with poor overall survival in HNSCC and breast cancer (6, 15). Down-regulation of ANO1 protein levels by RNAi in HNSCC, ESCC, prostate cancer, and breast cancer cells inhibits proliferation *in vitro* and *in vivo* by inhibiting activation of epidermal growth factor receptor and MAPK/AKT-signaling pathways and thus establishes ANO1 as an important survival factor in these cells (6, 7, 15). Furthermore, ANO1 has

Crystallographic data (excluding structure factors) have been deposited with the Cambridge Crystallographic Data Centre as supplementary publication number CCDC 939945.

✂ Author's Choice—Final version full access.

¹ Present address: Schrödinger, Inc., Cambridge, MA 02139.

² To whom correspondence should be addressed: Novartis Institutes for Biomedical Research, 500 Technology Square, Cambridge, MA 02139. Tel.: 617-871-7209; Fax: 617-871-5783; E-mail: alex.gaither@novartis.com.

³ The abbreviations used are: HNSCC, head and neck squamous carcinoma; ESCC, esophageal squamous carcinoma; CaCC, calcium-activated chloride channel; ER, endoplasmic reticulum; PGG, pentagalloyl glucose; BFA, brefeldin A.

CaCC_{inh}-A01 Promotes Degradation of ANO1

been implicated to regulate tumor cell motility and metastasis via interaction with the cytoskeletal proteins of the ezrin/radixin/moesin family (16). Therefore, ANO1 may represent a promising target for cancer therapy.

The identification of inhibitors targeting the CaCC activity of ANO1 suggests that biochemical inhibition of ANO1 function is feasible and that targeted modulation could be of therapeutic benefit. However, many of the reported ANO1 inhibitors are natural products with a broad specificity and show activity only in the high micromolar range (17). Screens have identified more potent and more specific inhibitors of ANO1 (17–20). CaCC_{inh}-A01 has been shown to inhibit ANO1-dependent chloride conductance in cells and to decrease proliferation of ANO1-dependent cell lines (6, 17). More recently, T16A_{inh}-A01, another small molecule inhibitor of ANO1 biochemical activity, has been reported (18). However, direct binding of neither T16A_{inh}-A01 nor CaCC_{inh}-A01 to ANO1 has been shown, and the mechanism of inhibition is still unknown. It remains unclear how inhibition of a transient chloride current results in inhibition of proliferation over a multiple-day time course.

We sought to explore the mechanism of CaCC_{inh}-A01-dependent inhibition of cell proliferation using a combined experimental and *in silico* approach. We show that CaCC_{inh}-A01 but not T16A_{inh}-A01 inhibits proliferation of ANO1-amplified cell lines, indicating that inhibition of ANO1 biochemical activity was not sufficient to decrease cell proliferation because both inhibitors inhibited the channel activity of ANO1. Rather we show that CaCC_{inh}-A01 inhibits cell proliferation by promoting endoplasmic reticulum (ER)-associated proteasomal degradation of ANO1. By performing structure-activity analysis based on the x-ray crystal structure of CaCC_{inh}-A01, we developed a pharmacophore model and identified new inhibitors of ANO1-dependent cell proliferation, all of which facilitated ANO1 degradation. Our data demonstrate that inhibition of ANO1 activity is not sufficient to inhibit proliferation of ANO1-amplified cell lines, indicating that both ANO1 channel activity and ANO1 protein are required for its role in cancer. Furthermore, we have shown the utility of *in silico* pharmacophore modeling methods to guide the understanding of biological phenomena involving proteins that have only limited structural information available and are not readily accessible via experimentation.

EXPERIMENTAL PROCEDURES

In Silico—Virtual screens and pharmacophore alignments were performed with the Cresset suite of programs, including FieldAlign and FieldScreen (21, 22). Structure-activity relationship and quantitative structure-activity relationship analysis were performed using Schrödinger's cheminformatics program, Canvas (Canvas, version 1.5, Schrödinger, LLC, New York) (23, 24). Surface area and volume calculations were computed within Schrödinger's Maestro (Maestro, version 9.3, Schrödinger).

Quantitative Structure-Activity Relationship—The 25 most potent compounds were considered. The data were split randomly into 75% training and 25% testing subsets. The most robust model proved to be the two-dimensional multiple linear regression model. R^2 for the training set and the Q^2 for the test set were both about 0.75, and the S.E. in the modeled value of

the hit score was 0.06–0.07. Cell culture was performed as described previously (6).

Compounds—T16A_{inh}-A01 (Tocris), digallic acid (Toronto Research Chemicals), pentagalloyl glucose (PGG) (Sigma-Aldrich), tannic acid (Bosche Scientific), CaCC_{inh}-NV2 and -NV7, brefeldin A (BFA), chloroquine, MG132 (Sigma-Aldrich), cycloheximide (Calbiochem), CaCC_{inh}-A01 (Specs), CaCC_{inh}-NV4 (ChemDiv), and all other compounds obtained from our internal archive were dissolved in DMSO to a final concentration of 10 mM. If not noted otherwise, cells were treated with 10 μ M compound.

Crystal Structure Determination and Refinement of CaCC_{inh}-A01—The Ca²⁺ complex of CaCC_{inh}-A01 was prepared by adding 10 μ l of a saturated solution of Ca(OH)₂ in MeOH to a solution of 1 mg of CaCC_{inh}-A01 in 200 μ l of EtOH and letting the solvents evaporate at ambient temperature. Colorless crystals were obtained within 1 day. Diffraction data were collected with a Bruker AXS SMART 6000 CCD detector on a three-circle platform goniometer with Cu(K α) radiation ($\lambda = 1.54178$ Å) from a Microstar rotating anode generator equipped with Incoatec multilayer mirrors. A semiempirical absorption correction was applied, based on the intensities of symmetry-related reflections measured at different angular settings (maximum and minimum transmission 0.8494 and 0.7290). The structure was solved by dual-space recycling methods and refined on F² with the SHELXTL suite of programs.

CaCC_{inh}-A01 crystallizes in the triclinic space group P-1 as a hexamer with 0.33 eq of ethanol. The (disordered) ethanol molecule is coordinating Ca₂₅. The disorder was modeled by refining two different orientations (*a*, *b*) with a 0.55 (*a*) to 0.45 (*b*) distribution. Two residual electron density peaks close to the inversion center were interpreted as half a methanol molecule. Although the respective hydrogen atoms at C56 and O57 were calculated in idealized positions, they interfere with H2 from one of the furane moieties. This might indicate that the residual electron density could also be interpreted as partially occupied water sites. All three CaCC_{inh}-A01 ligands are disordered in the region of the *tert*-butyl group. This disorder was modeled by refining two different orientations (*a*, *b*) with the following distributions (*a*:*b*): 0.73:0.27 in ligand 1, 0.62:0.38 in ligand 2, and 0.64:0.36 in ligand 3. Bond lengths, angles, and displacement parameters of all minor occupancy orientations were restrained to be similar to those of the major occupancy orientations. For the major occupancy orientation atoms, anisotropic displacement parameters were used, and for the minor occupancy orientation atoms, isotropic displacement parameters were used (except for the ethanol molecule). Hydrogen atoms were calculated in idealized positions and refined using a riding model. Final data: C₁₁₃ H₁₄₄ N₆ O₃₁ S₆ Ca₃; $M_r = 2394.94$ (calculated for hexamer of CaCC_{inh}-A01 with 3 Ca²⁺, 2 ethanol, 1 methanol), crystal size 0.12·0.08·0.06 mm³ (grown from methanol/ethanol), triclinic, space group P-1 (No. 2) with $a = 14.329(4)$, $b = 15.048(4)$, $c = 15.612(4)$ Å, $\alpha = 69.862(14)^\circ$, $\beta = 72.486(13)^\circ$, $\gamma = 79.705(12)^\circ$, $V = 3003.4(14)$ Å³, $Z = 1$, $D_c = 1.324$ g·cm⁻³, $\mu = 2.811$ mm⁻¹, $F(000) = 1268$, 64,238 reflections measured, 10,825 independent, $R_{int} = 0.0392$, $3.12^\circ < \theta < 68.33^\circ$, $T = 100(2)$ K, 832 parameters, 687 restraints, $R_1 = 0.0395$, $wR_2 = 0.1062$ for 9408 reflections with $I > 2\sigma(I)$, $R_1 =$

0.0472, $wR_2 = 0.1145$ for all 10,825 data, GoF = 1.030, restrained GoF = 1.038, res. el.dens. = $+0.59/-0.36 \text{ e} \cdot \text{\AA}^3$.

Copy number analysis and quantitative PCR were performed as described previously (6). Cell viability and colony formation assays were performed as described (6). Cell viability was determined after a 72-h treatment with compound. Colonies were stained after 10–14 days. Compounds were rank-ordered by hit score.

The hit score is given by Equation 1,

$$\text{hit score} = \frac{1}{6} \sum_{1,5,20\mu\text{M}} \sqrt{(I_1 - 1)^2 + (I_2 - 1)^2 + S_1^2 + S_2^2} \quad (\text{Eq. 1})$$

where I and S are the average relative cell viability (normalized to DMSO-only-treated cells), with I_1 and I_2 as the two ANO1 inhibition-insensitive cell lines (Te1 and KYSE150) and S_1 and S_2 as the two CaCC_{inh}-A01-sensitive and ANO1-dependent cell lines (Te11 and FaDu). Because the assays were run at varying concentrations of inhibitor (1, 5, and 20 μM), the summation is taken over the results obtained at all three concentrations. CaCC_{inh}-A01 resulted in a hit score of 0.40. Compounds with a hit score smaller than $0.40 + 10\%$ (hit score <0.44) were classified as a “hit” in subsequent assays.

Generation of stable cell lines expressing shRNAs was performed as described (6, 25, 26). Native PAGE was performed as described (25, 26). Cross-linking was performed as described (27).

Immunoprecipitation—Cells were lysed in radioimmune precipitation buffer (Cell Signaling), and $\sim 500 \mu\text{g}$ of total protein was incubated with an anti-ubiquitin antibody (Millipore, FK2) for 1 h at 4 °C. Antibodies were precipitated using Protein G-coated Dynabeads (Invitrogen), and bound protein was eluted in Laemmli buffer (Invitrogen) for 10 min at 70 °C. Western blotting was performed as described (6).

Immunofluorescence—Cells were fixed in 4% paraformaldehyde in PBS for 20 min at room temperature; incubated in 0.1% SDS/PBS for 5 min; blocked in 5% BSA, PBS, 0.3% Triton X-100 for 1 h at room temperature; and incubated in primary antibody (anti-ANO1, SP31, Abcam, 1:200; anti- β -catenin, Cell Signaling, 1:500) overnight in 3% BSA, PBS, 0.3% Triton X-100. Binding of the primary antibody was visualized by Alexa 594- or 488-labeled secondary antibodies (1:3000; Invitrogen). Coverslips were mounted, and nuclei were stained with DAPI (Vectashield, Vector Labs). Images were taken with an Olympus IX-81 inverted microscope (Olympus). Cell cycle analysis was performed as described previously (6).

QPatch—Whole-cell currents were measured using planar (QPatch, Sophion) patch clamp electrophysiology (28), as described (6).

RESULTS

Inhibition of ANO1 Activity Is Not Sufficient to Inhibit ANO1-dependent Cell Proliferation—ANO1 is amplified and highly expressed in HNSCC, ESCC, and breast cancer (6, 7, 15). ANO1 is an important oncogenic survival factor in these cancers, and RNAi-mediated knockdown of ANO1 in Te11 (HNSCC) and

FaDu (ESCC) cells diminished cell proliferation (6). Treatment of ANO1-amplified Te11 and FaDu cells with the ANO1 inhibitor CaCC_{inh}-A01 decreased colony formation and cell viability over a >72 -h time course. Consistent with ANO1 being the primary target of this compound, cells without ANO1 amplification and low expression of ANO1 (e.g. KYSE150, Te1, and HeLa) were found to be insensitive to CaCC_{inh}-A01 (Fig. 1, A–C, and Table 1). Interestingly, T16A_{inh}-A01 and digallic acid did not inhibit the proliferation of ANO1-dependent cell lines, although both compounds have been reported to inhibit ANO1 activity (Fig. 1, E and F) (18). These data suggest that inhibition of ANO1 activity alone is not sufficient to inhibit ANO1-dependent cell proliferation.

Small Molecule Crystal Structure of CaCC_{inh}-A01 Shows Calcium Binding—To understand the mechanism of CaCC_{inh}-A01 activity, we performed structure-activity analysis around CaCC_{inh}-A01. We set out to explore the presence of a carboxylic acid on CaCC_{inh}-A01 because this functional group is a putative chelator of metal ions, including calcium. We speculated that chelation of calcium may play a role in the activity of CaCC_{inh}-A01 because ANO1 is a calcium-activated chloride channel. In order to explore this hypothesis, we asked what form CaCC_{inh}-A01 would take when crystallized in the presence of calcium. An in-house x-ray crystal structure shows a hexameric unit cell of CaCC_{inh}-A01 in the P-1 space group chelating three calcium atoms (Fig. 2A). Within the structure, it is evident that there is a symmetric, intercalated CaCC_{inh}-A01 trimer architecture centered on a central calcium atom inversion center, suggesting that chelation of calcium may be important for the activity of CaCC_{inh}-A01. CaCC_{inh}-A01 is known to not affect intracellular calcium levels (17); however, because ANO1 is regulated by multiple calcium-dependent mechanisms (29), we speculated whether the ability of the compound to chelate local stores of calcium was sufficient to exhibit an effect on ANO1-dependent cell proliferation. We tested 70 known calcium chelators for an effect on cell proliferation in two ANO1-dependent (Te11, FaDu) and two ANO1-independent (KYSE150, Te1) cell lines. None of the calcium chelators tested inhibited ANO1-dependent cell proliferation, suggesting that calcium chelation alone is not sufficient to account for the activity of CaCC_{inh}-A01 in ANO1-amplified cell lines (data not shown). In addition, we have tested the effect of EGTA-AM (a cell membrane-permeable form of EGTA) for an effect on the proliferation of Te11, FaDu, KYSE150, and Te1 cells. EGTA-AM inhibited proliferation of all four cell lines with an IC_{50} of $\sim 10 \mu\text{M}$, indicating that it acts via an ANO1-independent mechanism. This further corroborates our finding that the calcium chelation functionality of CaCC_{inh}-A01 is important but not sufficient for the compound's activity on proliferation seen in ANO1-amplified cell lines.

Chelating Functionality Is Necessary for CaCC_{inh}-A01 Activity—We speculated that calcium chelation and a specific binding interaction of CaCC_{inh}-A01 with ANO1 together drive potency. Accordingly, we sought to identify additional compounds that shared those pharmacophoric features of CaCC_{inh}-A01. An *in silico* screen was performed, where a CaCC_{inh}-A01 crystallographic monomer was used as a template (Fig. 2, B and C). A total of 170 compounds with pharmacophore features

CaCC_{inh}-A01 Promotes Degradation of ANO1

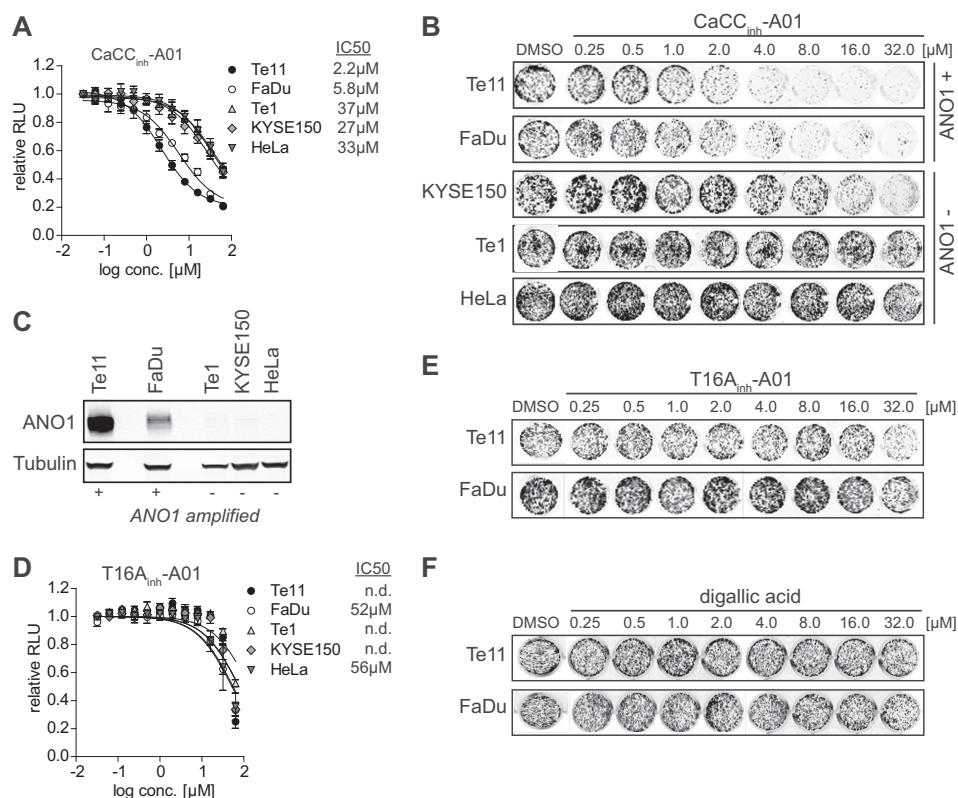


FIGURE 1. Inhibition of ANO1-dependent chloride conductance is not sufficient to inhibit ANO1-dependent cell proliferation. *A*, effect of CaCC_{inh}-A01 on proliferation of the indicated cell lines (mean \pm S. E. (error bars), $n > 3$). Cell viability was determined after 72 h of treatment with the indicated compounds or solvent. *B*, effect of CaCC_{inh}-A01 on colony formation of the indicated cell lines. Cells were seeded at low density and treated with the indicated compounds or solvent for 10–14 days. Colonies were stained using crystal violet. Representative images of stained colonies in a 24-well plate are shown. *C*, ANO1 expression was examined in the indicated cell lines by Western blotting. Representative blots are shown. *D*, effect of T16A_{inh}-A01 on proliferation of the indicated cell lines (mean \pm S.E., $n > 3$) analyzed as in *A*. *E* and *F*, effect of T16A_{inh}-A01 (*E*) or digallic acid (*F*) on colony formation of the indicated cell lines, analyzed as in *B*. RLU, relative light units.

TABLE 1

IC₅₀ values for inhibition of cell viability by CaCC_{inh}-A01 in correlation with ANO1 amplification status

Data represent the mean of three independent experiments. NA, non-amplified.

Cell line	Copy no. ANO1	IC ₅₀ CaCC _{inh} -A01
		μM
FaDu	14	8.5
KYSE140	4	8.0
KYSE510	6	3.1
Te11	9	2.9
Te6	9	2.5
Hek293	NA	>25
HeLa	NA	>25
KYSE150	NA	>25
KYSE450	NA	16
KYSE70	NA	>25
Te1	NA	16
Te9	NA	17

similar to those of CaCC_{inh}-A01 were identified and tested for their effect on ANO1-dependent cell proliferation (data of most the potent inhibitors are shown in Table 2, CaCC_{inh}-NV1–3). The compounds identified in this screen represented numerous potential chelators, including carboxylates, nitriles, amides, and esters, yet only the carboxylate-containing molecules showed activity in ANO1-dependent cell proliferation assays. CaCC_{inh}-NV1, -NV2, and -NV3 decreased the proliferation of ANO1-dependent cell lines in a concentration-dependent manner and inhibited ANO1-dependent current in Te11 cells (Fig. 2, D–F).

To investigate whether the presence of a chelating group is necessary for a compound's potency, we performed an *in silico* screen using the CaCC_{inh}-A01 crystal structure, where the carboxylate was replaced by hydrogen before being used as the template, and tested the predicted compounds in our proliferation assay. None of the 64 compounds identified from this screen showed activity in our cellular assay despite their high degree of similarity to the template molecule (examples shown in Table 2, CaCC_{inh}-NV4–8). This supports the hypothesis that both the hydrophobic interaction (hydrophobic bulk, missing in CaCC_{inh}-NV5 and -NV8) and calcium chelation moiety (carboxylic acid, missing in CaCC_{inh}-NV4, -NV6, and -NV7) present in CaCC_{inh}-A01 are necessary for potency in cells. This is corroborated via *in silico* analysis. We developed a quantitative structure-activity relationship model to describe our hit score: $\text{hit_score} = -0.34 \cdot \text{acidic_hydrogens} + 0.019 \cdot \text{AlogP}$. Notably, the developed quantitative structure-activity relationship model employs only two descriptors, which count the number of carboxylic acids and describe hydrophobicity, illustrating the importance of these two attributes to the hit score. Activity cliff analysis further supported this finding. Thus, we describe the first pharmacophore model for inhibitors of ANO1-dependent cell proliferation.

CaCC_{inh}-A01 Pharmacophore Model Can Be Used to Identify Inhibitors of ANO1-dependent Cell Proliferation—We used our pharmacophore model to rationalize the observed differential

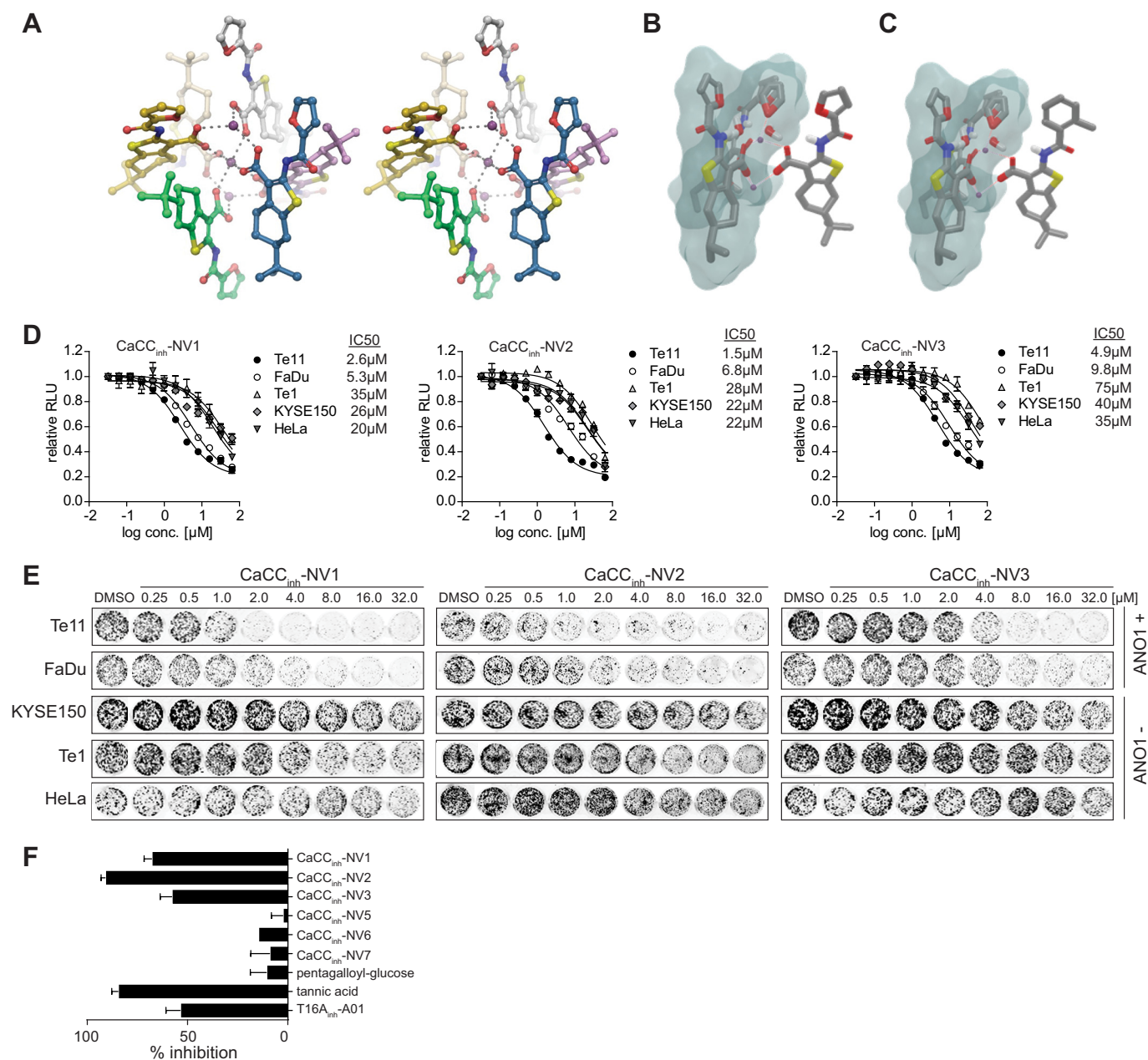


FIGURE 2. Virtual screening identifies novel inhibitors of ANO1-dependent cell proliferation. *A*, cross-eyed stereoisomer of the crystal structure of CaCC_{inh}-A01. No hydrogen atoms have been added, and water and solvent molecules have been omitted for clarity. Atoms are colored by element, with dark purple, red, blue, and yellow representing calcium, oxygen, nitrogen, and sulfur, respectively. The carbons are colored by molecule for clarity. *B* and *C*, crystal structure unit cell of CaCC_{inh}-A01 used to model CaCC_{inh}-A01 analogs. The excluded volume used from the crystal structure unit cell is shown outlined in blue, whereas the modeled compounds (*B*, CaCC_{inh}-A01; *C*, CaCC_{inh}-NV2) are shown on the right. The calcium ions are shown in purple. *D* and *E*, effect of CaCC_{inh}-NV1–3 on cell viability (*D*) and colony formation (*E*) of the indicated cell lines (mean \pm S.E. (error bars), $n = 4$; representative images of stained colonies in a 24-well plate are shown). *F*, relative inhibition of ANO1 currents in Te11 cells as compared with CaCC_{inh}-A01. The indicated compounds were tested at 30 μ M (mean \pm S.E., $n = 3$).

activity of T16A_{inh}-A01, digallic acid, and CaCC_{inh}-A01. Although all of these molecules inhibit the CaCC activity of ANO1 (18, 30), only CaCC_{inh}-A01 had an inhibitory effect on ANO1-dependent cell proliferation in tumor cells. T16A_{inh}-A01 lacks a carboxylic acid, a critical feature of the pharmacophore model (Fig. 3A). Digallic acid, although containing a carboxylic acid, lacks much of the hydrophobic bulk of CaCC_{inh}-A01 (Fig. 3B). Thus, both T16A_{inh}-A01 and digallic acid significantly deviate from our pharmacophore model. Given that digallic acid deviates from the pharmacophore by lacking hydrophobic bulk, we hypothesized that tannic acid,

being a glucose-linked pentamer of digallic acid with reported inhibitory activity on ANO1 (30), would fulfill this requirement and inhibit ANO1-dependent cell proliferation. In the alignment of tannic acid with the trimeric subunit of the hexameric crystal structure of CaCC_{inh}-A01, henceforth referred to as “trimer,” ~ 1.5 units of digallic acid overlap with each unit of CaCC_{inh}-A01 (Fig. 3, C and D). Thus, in tannic acid, the lack of bulk in the individual digallic acid units is compensated for by a larger numbers of these units. Furthermore, the glucosyl moieties of tannic acid align with the carboxylates of the CaCC_{inh}-A01 trimer, theoretically allowing for chelation of a cal-

CaCC_{inh}-A01 Promotes Degradation of ANO1

TABLE 2

Summary of the structural and biochemical characteristics for all newly identified molecules

Values of the hit score relative to that of CaCC_{inh}-A01 (in parentheses) and IC₅₀ are given.

Compound	Structure	Hit score	IC ₅₀ CTG	IC ₅₀ CFA	IC ₅₀ QPatch
CaCC _{inh} -A01		0.40	Te11: 2.2μM FaDu: 5.8μM Te1: 37μM KYSE150: 27μM HeLa: 33μM	Te11: 1.5μM FaDu: 6.8μM Te1: 28μM KYSE150: 22μM HeLa: 22μM	4.7 μM
CaCC _{inh} -NV1		0.40 (0.00)	Te11: 2.6μM FaDu: 5.3μM Te1: 35μM KYSE150: 26μM HeLa: 20μM	Te11: 1.1μM FaDu: 2.1μM Te1: 8.5μM KYSE150: 11μM HeLa: 20μM	15.8 μM
CaCC _{inh} -NV2		0.43 (0.03)	Te11: 1.5μM FaDu: 6.8μM Te1: 28μM KYSE150: 22μM HeLa: 22μM	Te11: 0.3μM FaDu: 0.7μM Te1: 7.3μM KYSE150: 13μM HeLa: 11μM	6.5 μM
CaCC _{inh} -NV3		0.43 (0.03)	Te11: 4.9μM FaDu: 9.8μM Te1: 75μM KYSE150: 40μM HeLa: 35μM	Te11: 2.1μM FaDu: 6.2μM Te1: 30μM KYSE150: 17μM HeLa: 27μM	19.2 μM
CaCC _{inh} -NV4		0.66 (0.26)	Te11: n.d. FaDu: 40μM Te1: 54μM KYSE150: 50μM HeLa: 35μM	Te11: 25μM FaDu: 16μM Te1: 23μM KYSE150: 9μM HeLa: 12μM	not active
CaCC _{inh} -NV5		0.69 (0.29)	Te11: n.d. FaDu: n.d. Te1: n.d. KYSE150: n.d. HeLa: n.d.	Te11: n.d. FaDu: n.d. Te1: n.d. KYSE150: n.d. HeLa: n.d.	not active
CaCC _{inh} -NV6		0.72 (0.32)	Te11: n.d. FaDu: n.d. Te1: n.d. KYSE150: n.d. HeLa: n.d.	Te11: n.d. FaDu: n.d. Te1: n.d. KYSE150: n.d. HeLa: n.d.	not active
CaCC _{inh} -NV7		0.73 (0.33)	Te11: n.d. FaDu: n.d. Te1: n.d. KYSE150: n.d. HeLa: n.d.	Te11: n.d. FaDu: n.d. Te1: n.d. KYSE150: n.d. HeLa: n.d.	not active
CaCC _{inh} -NV8		0.79 (0.39)	Te11: n.d. FaDu: n.d. Te1: n.d. KYSE150: n.d. HeLa: n.d.	Te11: n.d. FaDu: n.d. Te1: n.d. KYSE150: n.d. HeLa: n.d.	not active

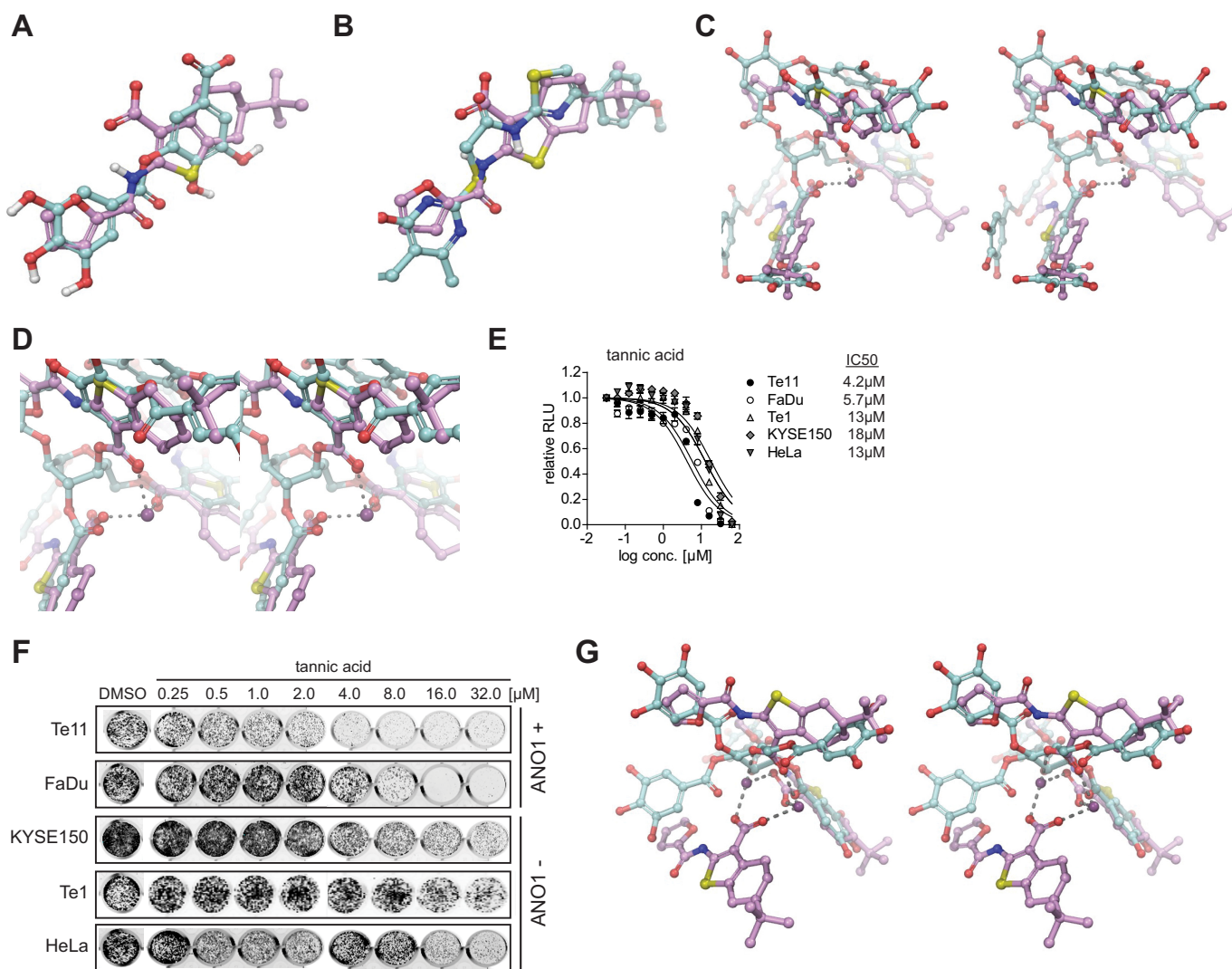


FIGURE 3. Tannic acid resembles CaCC_{inh}-A01 trimer, promotes degradation of ANO1, and inhibits ANO1-dependent cell proliferation. *A*, flexible ligand alignment of digallic acid with CaCC_{inh}-A01. Atoms are colored by element, with white, red, blue, and yellow representing hydrogen, oxygen, nitrogen, and sulfur, respectively. The carbons are colored by molecule for clarity, where turquoise and lilac correspond to digallic acid and CaCC_{inh}-A01, respectively. Note that only polar hydrogens are displayed for clarity. *B*, flexible ligand alignment of T16A_{inh}-A01 with CaCC_{inh}-A01. Atoms are colored by element with red, blue, and yellow representing oxygen, nitrogen, and sulfur, respectively. The carbons are colored by molecule for clarity, where turquoise and lilac correspond to T16A_{inh}-A01 and CaCC_{inh}-A01, respectively. Note that only polar hydrogens are displayed for clarity. *C*, cross-eyed stereoimage of flexible ligand alignment of tannic acid with the CaCC_{inh}-A01 crystallographic trimer. Atoms are colored as described in the legend to Fig. 2. The carbons are colored by molecule for clarity, where turquoise and lilac correspond to tannic acid and the CaCC_{inh}-A01 crystallographic trimer, respectively. One calcium ion of the CaCC_{inh}-A01 crystal structure is shown as a purple sphere. *D*, close-up cross-eyed stereoimage of flexible ligand alignment of tannic acid with the CaCC_{inh}-A01 crystallographic trimer. *E* and *F*, effects of tannic acid on cell proliferation (*E*) and colony formation (*F*) of the indicated cell lines (mean \pm S.E. (error bars), $n = 4$; representative images of stained colonies in a 24-well plate are shown). *G*, cross-eyed stereoimage of flexible ligand alignment of pentagalloyl glucose with the CaCC_{inh}-A01 crystallographic trimer. Atoms are colored by element, with dark purple, red, blue, and yellow representing calcium, oxygen, nitrogen, and sulfur, respectively. The carbons are colored by molecule for clarity, where turquoise and lilac correspond to pentagalloyl glucose and the CaCC_{inh}-A01 crystallographic trimer, respectively. Note that no hydrogens are displayed for clarity.

cium cation, potentially stabilizing the conformation. Therefore, tannic acid lies within the confines of our pharmacophore model. In agreement with our hypothesis, tannic acid indeed inhibited cell proliferation of ANO1-dependent cell lines (Fig. 3, *E* and *F*).

We tested the potency of another tannic acid analog shown to inhibit ANO1-dependent chloride currents, PGG (30). PGG does not align with the trimer of CaCC_{inh}-A01 (Fig. 3*G*) and did not show a specific effect on the proliferation of ANO1-dependent cells and showed a nonspecific inhibition of proliferation in all tested cell lines (data not shown). PGG is known to inhibit cell proliferation in tumor types that do not express ANO1, so its cytotoxic effect in tumor cells is not due to ANO1 inhibition

(31). Thus, we posit that the pharmacophore model for inhibitors also includes conglomeration of small molecules into a multimeric structure that resembles tannic acid, explaining the observed similarity in activity of these seemingly disparate molecules. The characteristics necessary for ANO1 inhibitors to exhibit an effect on ANO1-dependent cell proliferation can be described by our pharmacophore model.

CaCC_{inh}-A01 Decreases ANO1 Protein Levels—We then investigated the cellular mechanism underlying the inhibitory effect of CaCC_{inh}-A01 on proliferation of ANO1-expressing cells. Given that genetic knockdown of ANO1 decreases cell viability in Te11 and FaDu cells (6), we asked whether the bind-

CaCC_{inh}-A01 Promotes Degradation of ANO1

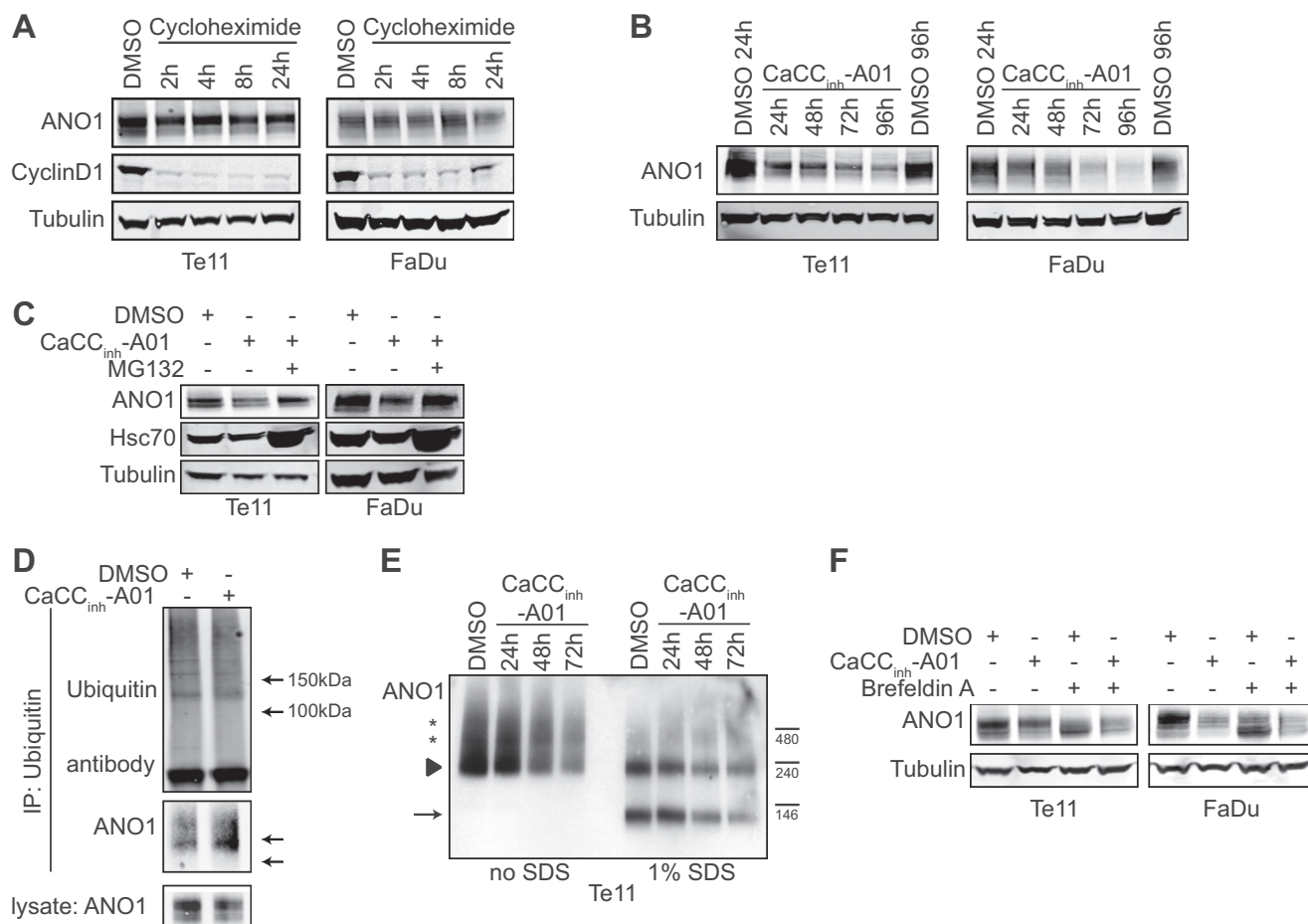


FIGURE 4. CaCC_{inh}-A01 promotes the endoplasmic reticulum-associated, proteasomal degradation of ANO1. *A*, analysis of ANO1 protein stability. Cells were treated for the indicated times with 50 μ M cycloheximide, and ANO1 protein levels were analyzed by Western blotting. Cyclin D1 was used for the activity of cycloheximide. Representative blots are shown. *B*, effects of CaCC_{inh}-A01 on ANO1 protein levels were examined by Western blotting after the indicated time of treatment with 10 μ M CaCC_{inh}-A01 or DMSO. Tubulin was used as a loading control. Representative Western blots are shown. *C*, effects of MG132 on CaCC_{inh}-A01-induced degradation of ANO1. Cells were pretreated with 10 μ M CaCC_{inh}-A01 for 6 h before the co-treatment with 20 μ M MG132 for an additional 18 h. Representative Western blots are shown. Hsc70 was used to control the effect of MG132. *D*, immunoprecipitation (IP) of mono- and polyubiquitinated proteins in Te11 cells treated with 10 μ M CaCC_{inh}-A01 or DMSO using an anti-ubiquitin antibody. Note the increase in the molecular weight for ANO1 due to ubiquitination. Representative Western blots are shown. *E*, representative Western blot of a blue native polyacrylamide gel is shown. Te11 cells were treated as indicated with 10 μ M CaCC_{inh}-A01 or DMSO. 1% SDS was added to the samples (lanes 6–9) prior loading to the gel. Arrow, expected size of ANO1 monomer; arrowhead, expected size of ANO1 dimer; stars, ANO1 multimers or complexes. *F*, effects of 10 μ M brefeldin A on CaCC_{inh}-A01-induced degradation of ANO1. Representative Western blots are shown.

ing of CaCC_{inh}-A01 to ANO1 might affect the expression or stability of the protein in addition to inhibiting its channel activity. Because the stability of ANO1 in cells has not been studied previously, we investigated the protein half-life of ANO1 in cells. Our results show that the half-life of ANO1 protein is greater than 24 h (Fig. 4A). In order to test for an effect of CaCC_{inh}-A01 on ANO1 expression or stability, Te11 and FaDu cells were treated with CaCC_{inh}-A01. ANO1 mRNA and protein levels were monitored over a time course by quantitative PCR and Western blotting, respectively. Treatment of Te11 and FaDu cells with CaCC_{inh}-A01 had no effect on ANO1 mRNA levels (data not shown) but led to a decrease in ANO1 protein levels in a time-dependent manner, indicating post-transcriptional regulation of ANO1 protein levels after CaCC_{inh}-A01 treatment (Fig. 4B).

CaCC_{inh}-A01 Promotes Proteasomal Degradation of ANO1—Given the long half-life of ANO1, we speculated that CaCC_{inh}-A01 might affect ANO1 protein levels by inducing degradation of the protein via the lysosome- or proteasome-dependent deg-

radation pathway. Whereas inhibition of lysosomal degradation using chloroquine had no effect on ANO1 protein levels in Te11 or FaDu cells (data not shown), inhibition of the proteasome with MG132 prevented ANO1 degradation after CaCC_{inh}-A01 treatment in both cell types (Fig. 4C). Consistent with this result, we found that CaCC_{inh}-A01 treatment increased the ubiquitination of ANO1 (Fig. 4D). Taken together, these data provide evidence that CaCC_{inh}-A01 promotes proteasome-dependent degradation of ANO1.

CaCC_{inh}-A01 Does Not Affect the Dimerization of ANO1—We then investigated the mechanism by which CaCC_{inh}-A01 induces proteasome-dependent degradation of ANO1. We hypothesized that CaCC_{inh}-A01 may increase degradation of ANO1 by affecting its stability (e.g. by disrupting critical protein-protein contacts), compromising the structure of the protein, and leaving the protein vulnerable to degradation. ANO1 has been shown to form dimers when overexpressed in HEK293 cells (25, 26, 32), and we hypothesized that CaCC_{inh}-A01 might interfere with the dimerization of ANO1. To explore this

hypothesis, we tested the effects of CaCC_{inh}-A01 on the stability of the dimeric form of ANO1 and on the interaction of ANO1 with other proteins by performing non-denaturing blue native polyacrylamide gel electrophoresis followed by Western blot analysis for ANO1. Under non-denaturing conditions, an ANO1 antibody stained for several bands (Fig. 4E), including the main signal observed around 240 kDa, representing dimeric ANO1. Several bands of higher molecular weight were detectable in lysates of Te11 cells, indicating the existence of oligomers or complexes of ANO1 with other proteins. Partial denaturation of the natively extracted ANO1 by the addition of 1% SDS to the sample resulted in a decrease of the 240 kDa band and disappearance of higher order complexes. A faster migrating band around 120 kDa was detected, representing the monomeric form of ANO1. Treatment of Te11 cells with CaCC_{inh}-A01 decreased total ANO1 protein levels but did not affect the quaternary structure of total ANO1 protein in the cells. Similar results were obtained in FaDu cells (data not shown). Consistently, treatment of Te11 and FaDu cells with CaCC_{inh}-A01 had no effect on the ratio between the monomeric and dimeric form of ANO1 on the cell membrane after cross-linking with the cell-impermeable cross-linker BS3 but consistently decreased total ANO1 protein levels (data not shown). These results provide evidence that ANO1 forms dimeric and multimeric complexes under endogenous expression in tumor cells and that the formation of these complexes is not affected by CaCC_{inh}-A01.

CaCC_{inh}-A01 Facilitates ER-associated, Proteasomal Turnover of ANO1—Next, we tested whether CaCC_{inh}-A01 treatment induces the internalization from the plasma membrane and the transfer of ubiquitinated ANO1 to the proteasome. Immunofluorescence staining of ANO1 after treatment of Te11 and FaDu cells with CaCC_{inh}-A01 did not reveal any vesicular staining of ANO1 and rather caused a gradual overall decrease of total ANO1 staining intensity in the cells (data not shown). This observation led us to hypothesize that CaCC_{inh}-A01 interferes with the turnover of ANO1 protein by facilitating the degradation of the intracellular pool of ANO1. To test this hypothesis, we treated Te11 and FaDu cells with BFA (33, 34), which led to a shift in the molecular weight for ANO1, representing the partially glycosylated, non-(Golgi)matured form of ANO1 and indicating that ANO1 undergoes intracellular recycling by retrograde transport (Fig. 4F). To test whether the CaCC_{inh}-A01-dependent turnover of ANO1 occurs in the ER or a post-Golgi compartment, we treated the cells with a combination of BFA and CaCC_{inh}-A01. Treatment of Te11 and FaDu cells with CaCC_{inh}-A01 in the presence of BFA led to a decrease in ANO1 protein levels as compared with BFA treatment alone (compare lanes 3 and 4 and lanes 7 and 8). These data demonstrate that degradation of ANO1 still appears in the presence of BFA, indicating that the degradation occurs in a pre-Golgi compartment. Taken together, these results suggest that CaCC_{inh}-A01 interferes with the intracellular turnover of ANO1 by promoting the ER-associated, proteasomal degradation of ANO1.

CaCC_{inh}-A01 Inhibits Cell Proliferation by Reducing ANO1 Protein Levels—Given that RNAi-mediated knockdown of ANO1 decreases cell viability in Te11 and FaDu (6), we hypothesized that the inhibitory effect of CaCC_{inh}-A01 on cell proliferation

results from compound-induced reduction in ANO1 protein levels. Consistent with this, all of our newly identified inhibitors of ANO1-dependent cell proliferation (CaCC_{inh}-NV1, CaCC_{inh}-NV2, and CaCC_{inh}-NV3) as well as tannic acid decreased ANO1 protein levels, whereas their structurally similar but inactive counterparts (CaCC_{inh}-NV4, CaCC_{inh}-NV5, CaCC_{inh}-NV6, CaCC_{inh}-NV7, and CaCC_{inh}-NV8) and pentagalloyl glucose did not (Fig. 5, A–D). Intriguingly, treatment with T16A_{inh}-A01 or digallic acid did not affect ANO1 protein levels, correlating with their lack of effect on ANO1-dependent cell proliferation. This led us to hypothesize that CaCC_{inh}-A01 inhibits ANO1-dependent cell proliferation by reducing ANO1 protein levels. Therefore, removal of CaCC_{inh}-A01 should lead to recovery of ANO1 protein levels and resume cell proliferation. To test this hypothesis, we treated Te11 and FaDu cells for 72 h with CaCC_{inh}-A01, followed by washout of CaCC_{inh}-A01 and incubation of the cells in normal growth medium. Samples for cell cycle and Western blot analysis of ANO1 were taken every 24 h, and cell viability was monitored. Treatment of Te11 and FaDu cells with CaCC_{inh}-A01 reduced protein levels of ANO1, arrested the cells in the G₁ phase of the cell cycle, and led to pronounced inhibition of cell growth in both cell lines. Consistent with our hypothesis, washout of CaCC_{inh}-A01 completely rescued ANO1 protein levels and restored cell viability (Fig. 5, E–G). Notably, CaCC_{inh}-A01 also reduced ANO1 protein levels in Te9, KYSE140, and KYSE510 cells (Fig. 5H). Taken together, these data provide strong evidence that CaCC_{inh}-A01 inhibits proliferation of ANO1-amplified cancer cell lines by decreasing ANO1 protein levels, suggesting that both ANO1-activity and protein are necessary for its role as a survival factor in cancer.

To further investigate the dual role of ANO1 in cancer, we generated CaCC_{inh}-A01-resistant Te11 cell pools by culturing the cells in 10 μM CaCC_{inh}-A01 (~4-fold IC₅₀) for >3 months. Proliferation of the resistant Te11 cell pools was significantly less sensitive to CaCC_{inh}-A01 and to all of the newly identified inhibitors of ANO1-dependent cell proliferation (CaCC_{inh}-NV1, CaCC_{inh}-NV2, and CaCC_{inh}-NV3) as compared with parental, wild type Te11 cells (Fig. 6, A and B) and showed an IC₅₀ similar to that of ANO1-negative cells (Fig. 1A). There was no difference in sensitivity to ANO1-independent inhibition of proliferation (data not shown). Genomic sequencing of the ANO1 locus did not reveal any acquired mutations in ANO1 in the resistant cell pool (data not shown). ANO1 protein levels in Te11 wild type cells and the CaCC_{inh}-A01-resistant cell pool were similar (Fig. 6C). QPatch measurements did not reveal a significant difference in ANO1 chloride currents but showed that ANO1-dependent currents were still inhibited by CaCC_{inh}-A01 in the resistant cell pool with an IC₅₀ similar to that of the parental cells (Fig. 6, D and E), further supporting our hypothesis that sustained inhibition of ANO1 channel activity is not sufficient to diminish cell proliferation. Furthermore, treatment with CaCC_{inh}-A01 decreased ANO1 protein levels in Te11 parental, wild type cells but did not affect ANO1 protein levels in the CaCC_{inh}-A01-resistant cell pool (Fig. 6C), providing an explanation for the lack of effect on cell proliferation and demonstrating that promotion of ANO1 degradation is responsible for the effect of CaCC_{inh}-A01 on proliferation of ANO1-

CaCC_{inh}-A01 Promotes Degradation of ANO1

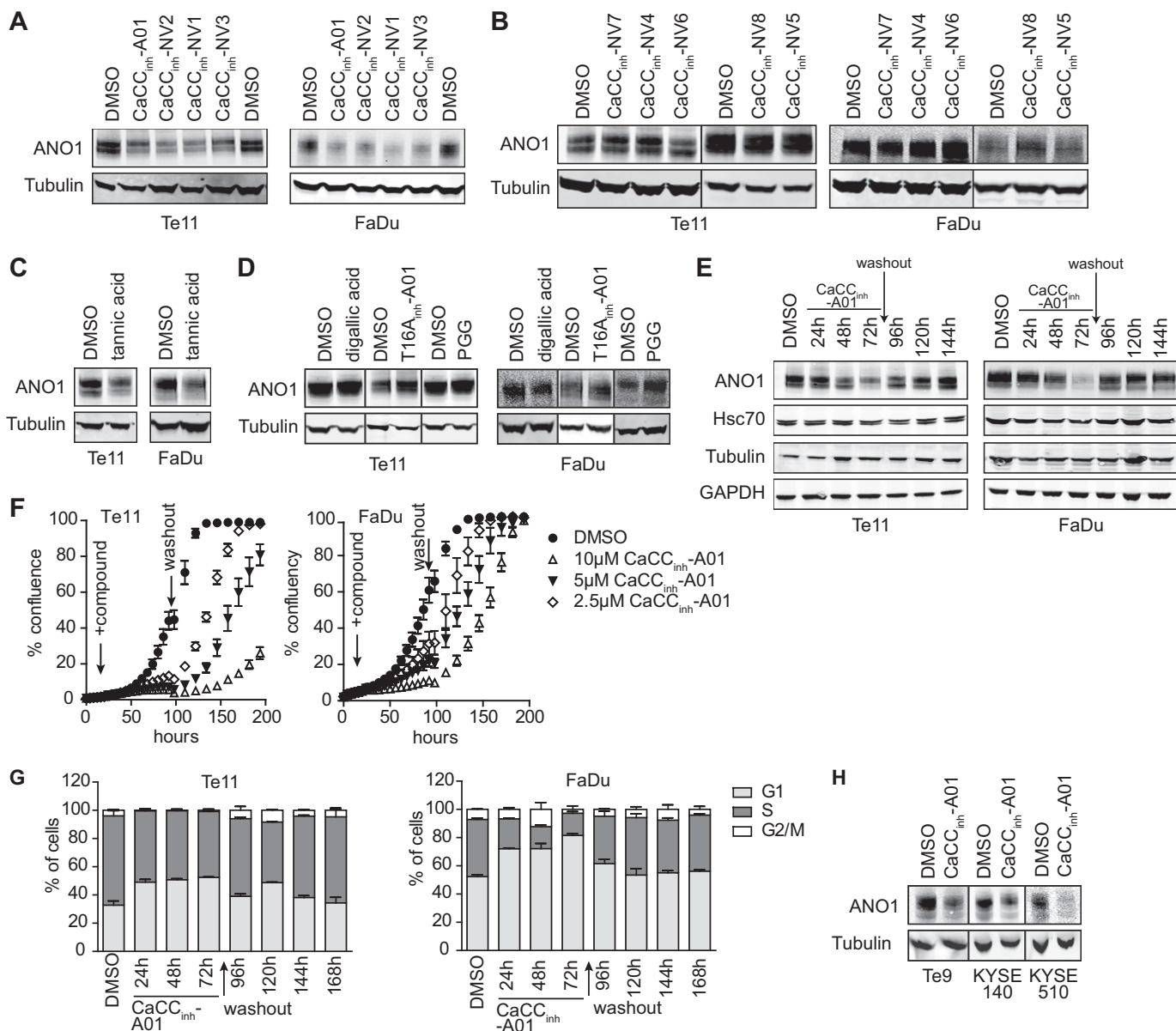


FIGURE 5. CaCC_{inh}-A01 inhibits proliferation by promoting degradation of ANO1. *A*, effects of CaCC_{inh}-NV1–3 on ANO1 protein levels were examined by Western blotting after 72 h of treatment with 10 μ M compound or DMSO. Representative Western blots are shown. *B*, effects of CaCC_{inh}-NV4–8 on ANO1 protein levels examined as in *A*. *C* and *D*, effects of tannic acid, digallic acid, T16A_{inh}-A01, and PGG on ANO1 protein levels examined as in *A*. *E*, effect of CaCC_{inh}-A01 washout on ANO1 protein levels assessed as described in *A*. *F*, Te11 and FaDu cell proliferation in the presence and after washout of the indicated concentrations of CaCC_{inh}-A01 or DMSO was monitored using the Incucyte system (mean \pm S.E. (error bars), $n = 4$). *G*, cell cycle analysis of Te11 and FaDu cells in the presence of and after washout of the indicated concentrations of CaCC_{inh}-A01 or DMSO. Cells were stained with propidium iodide, and DNA content was analyzed by FACS (mean \pm S.E., $n = 3$). *H*, effects of CaCC_{inh}-A01 on ANO1 protein levels were examined in the indicated cell lines by Western blotting after 72 h of treatment with 10 μ M CaCC_{inh}-A01 or DMSO. Representative Western blots are shown.

amplified cancer cells. In order to test whether the CaCC_{inh}-A01-resistant cells were still dependent on ANO1 or whether the cells had developed an alternative mechanism that made them ANO1-independent and thus resistant to CaCC_{inh}-A01, we generated CaCC_{inh}-A01 cell lines stably expressing doxycycline-inducible shRNAs against ANO1 (Fig. 6F, #1 and #2) or a non-targeting control (NT). Treatment of shRNA#1/#2-expressing cell lines with doxycycline diminished ANO1 expression, whereas doxycycline had no effect on ANO1 expression in the NT control-expressing cell line (Fig. 6F). As shown in Fig. 6G, the newly generated stable shRNA lines retained resistance to CaCC_{inh}-A01. To test the hypothesis that the resistant cells

were still dependent on ANO1 expression, we treated the shRNA-expressing Te11-RES cells with doxycycline and measured cell viability in a colony formation assay. Knockdown of ANO1 led to a significant inhibition of cell viability as detected by a decrease in colony formation (Fig. 6H). This finding demonstrates that CaCC_{inh}-A01-resistant cells still require ANO1 protein for proliferation and is consistent with our model that the observed CaCC_{inh}-A01-resistance in Te11-RES can be explained by the lack of degradation of ANO1 rather than the occurrence of alternative, ANO1-independent resistant mechanisms. In summary, our data demonstrate that degradation of ANO1 rather than inhibition of ANO1 channel activity is crit-

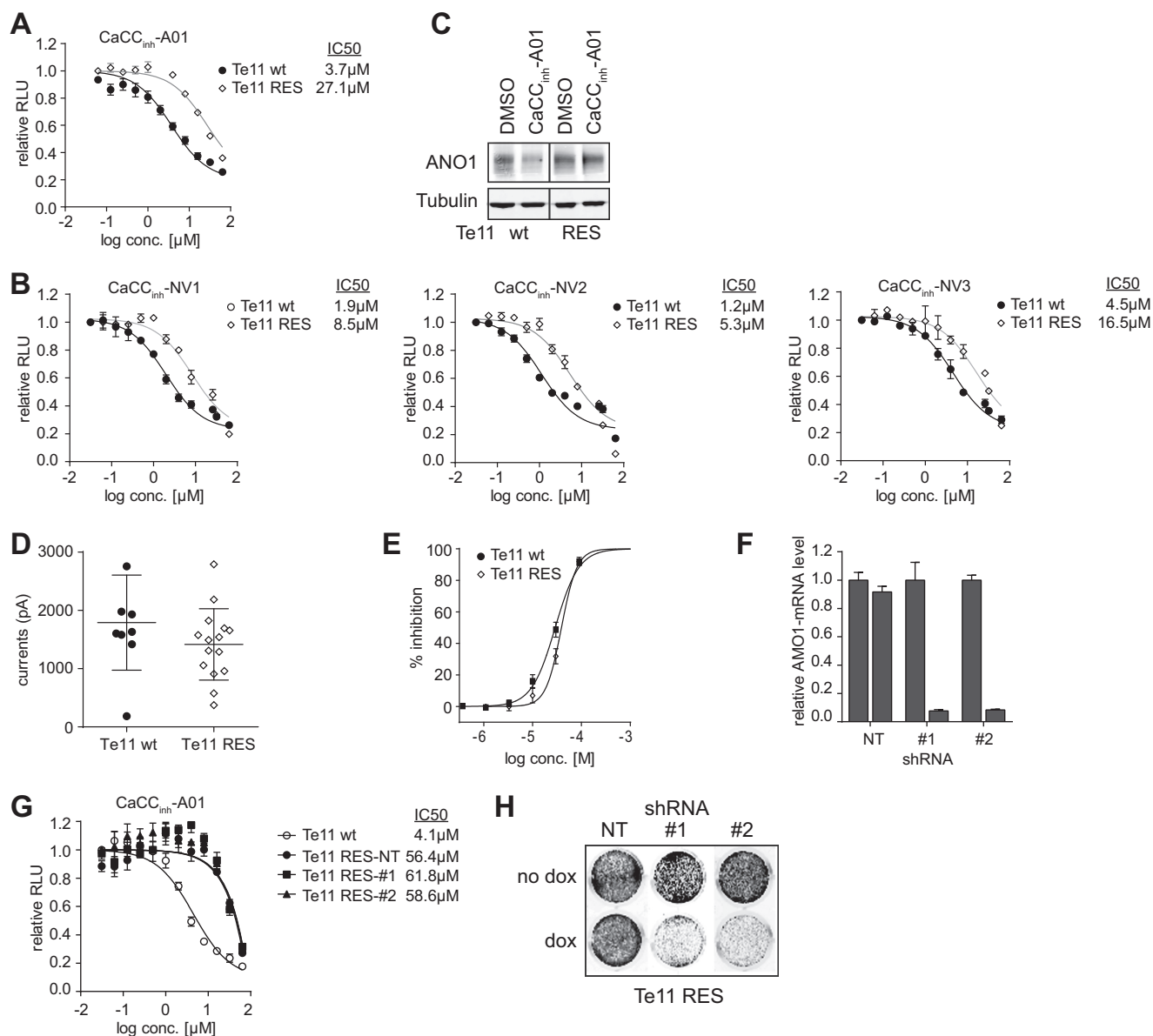


FIGURE 6. Resistance to CaCC_{inh}-A01-promoted degradation of ANO1 rescues CaCC_{inh}-A01-dependent inhibition of cell proliferation. *A* and *B*, effects of CaCC_{inh}-A01 (*A*) and analogs (*B*) on proliferation of parental Te11 cells and CaCC_{inh}-A01-resistant Te11 cell pools (mean \pm S.E. (error bars), $n = 4$, 72-h treatment). *C*, effects of CaCC_{inh}-A01 on ANO1 protein levels in parental Te11 cells and CaCC_{inh}-A01-resistant Te11 cell pools. Representative Western blots are shown. *D*, ANO1-like currents in Te11 WT and RES cells as assessed using QPatch (mean \pm S.E., $n = 10$). *E*, percentage of inhibition of ANO1-like currents in Te11 WT and RES cells at the indicated concentrations of CaCC_{inh}-A01 (mean \pm S.E., $n = 4$). *F*, relative mRNA-level of ANO1 of Te11-RES cells stably expressing doxycycline-inducible shRNA against ANO1 (#1 and #2) or a non-targeting control (NT) after 72-h treatment with or without doxycycline as determined by quantitative PCR. Data are normalized to the respective non-doxycycline-treated control and represent the mean \pm S.E., $n = 3$. *G*, effect of CaCC_{inh}-A01 on proliferation of parental Te11 cells and Te11-RES cells stably expressing shRNA as described in *F* (mean \pm S.E., $n = 3$, 72-h treatment). *H*, effect of ANO1 knockdown on colony formation of Te11-RES cells. Te11-RES cells stably expressing doxycycline-inducible shRNA against ANO1 or a non-targeting control were seeded in a 24-well plate colonies in a 24-well plate are shown. *RLU*, relative light units.

ical for the inhibition of ANO1-dependent cell proliferation in ANO1-amplified tumor cells.

DISCUSSION

ANO1 has been identified as an important survival factor in human cancers and contributes to HNSCC, ESCC, and breast cancer tumorigenesis, making it a promising therapeutic target (2–7). CaCC_{inh}-A01 has been shown to inhibit ANO1-dependent chloride conductance in cells and to decrease proliferation of ANO1-dependent cell lines (6, 17), but its mechanism of inhibition has remained elusive. In particular, it remains unclear how inhibition

of a transient chloride current results in inhibition of proliferation over a multiple-day time course. We explored the mechanism of CaCC_{inh}-A01-dependent inhibition of cell proliferation using a combined experimental and *in silico* approach. We show that CaCC_{inh}-A01 inhibits ANO1-dependent cell proliferation by reducing ANO1 protein levels in Te11 and FaDu cells. We found that CaCC_{inh}-A01 increased the ubiquitination of ANO1 and facilitated ER-associated, proteasomal degradation of ANO1 without affecting its dimerization. CaCC_{inh}-A01 interferes with the naturally occurring turnover processes of ANO1, providing an explanation for the observed slow kinetics of CaCC_{inh}-A01-in-

CaCC_{inh}-A01 Promotes Degradation of ANO1

duced loss of ANO1 protein. Our results are consistent with the observation that multiple ion channels have been shown to be regulated by endoplasmic reticulum-associated, ubiquitin-dependent degradation (29, 35–39).

Inhibitor-mediated degradation of proteins often originates in hydrophobic interactions of the molecule with protein. These interactions disrupt critical protein contacts, compromising the proteins' structure and eventually leading to degradation (40, 41). The inhibitors described herein and tannic acid contain a marked percentage of hydrophobic surface area. Approximately 21–29% of the surface area is highly hydrophobic (e.g. aromatic ring faces). In theory, the faces of the aromatic rings that constitute the hydrophobic surface area could π -stack with residues of ANO1 (e.g. tryptophan and tyrosine), ultimately leading to changes in the conformation of ANO1 and eventually degradation. Our model suggests that CaCC_{inh}-A01 and the analogs described herein bind to ANO1 and alter the structure and activity of ANO1, thereby facilitating the constitutive, ER-associated, proteasome-dependent turnover of ANO1. However, without a structure for ANO1, locating possible binding sites and validating this hypothesis remains a challenging goal for further studies. ANO1, being an eight-transmembrane helix protein and having no known homologs with solved structures, evades description with homology models. However, our model does not exclude binding of CaCC_{inh}-A01 to a second target that regulates ANO1 stability.

We report various inhibitors of ANO1-dependent cell proliferation, identified by structure-activity analysis of the structure of CaCC_{inh}-A01, all of which promote degradation of ANO1. A pharmacophore model was developed to describe compounds capable of facilitating ANO1 degradation and inhibiting ANO1-dependent cell proliferation. This model points to the importance of both the carboxylate and hydrophobic bulk as essential features of these compounds. Our model demonstrates that tannic acid promoted degradation of ANO1, whereas the closely related molecule PGG had no selective effect on ANO1-dependent cell proliferation. Importantly, we have shown the utility of *in silico* methods to guide a better understanding of the biological phenomena of the ANO1 channel when structural biological features of this protein are limiting.

Our data suggest that inhibition of ANO1-dependent chloride conductance is not sufficient to promote degradation of ANO1. T16A_{inh}-A01 and digallic acid had no effect on the proliferation of ANO1-dependent cells and did not reduce protein levels of ANO1, although both compounds inhibited ANO1-dependent chloride conductance with a similar potency as CaCC_{inh}-A01 (17, 18, 30). T16A_{inh}-A01 is a reported inhibitor of ANO1-dependent cell proliferation (15, 42). However, these experiments were performed at high concentrations of compound and resulted in weak effects on proliferation. These data suggest that inhibition of ANO1 channel activity alone is not sufficient to inhibit cell proliferation and that the reduction of ANO1 protein levels is requisite. ANO1 has been shown to interact with cytoskeletal proteins and to promote epidermal growth factor receptor/calcium/calmodulin-dependent protein kinase signaling in cancer cells (6, 15, 16), yet a detailed understanding of the involvement of ANO1 in these pathways

remains unclear. A recent study in dorsal root ganglia found ANO1 to be in a complex with the inositol 1,4,5-trisphosphate receptor 1, bradykinin receptor 2, the protease-activated receptor 2, and caveolin and to be tethered to juxtamembrane regions of the ER and suggests that a similar complex may exist in cancer cells (43). Future studies may show whether the compounds described herein may interfere with the complex, resulting in the destabilization and degradation of ANO1.

Using our combined experimental and computational techniques, we have made progress toward identification of potent and selective ANO1 inhibitors and uncovering the mechanism of how these inhibitors may work in cells. Our results provide impetus for gaining a deeper understanding of ANO1 modulation in cells, which could impact the treatment of ANO1-amplified cancers.

Acknowledgments—We thank William Forrester for critical reading of the manuscript and Derek Paisley for scientific advice and guidance.

REFERENCES

1. Jonkers, J., and Berns A. (2004) Oncogene addiction: sometimes a temporary slavery. *Cancer Cell* **6**, 535–8
2. West, R. B., Corless, C. L., Chen, X., Rubin, B. P., Subramanian, S., Montgomery, K., Zhu, S., Ball, C. A., Nielsen, T. O., Patel, R., Goldblum, J. R., Brown, P. O., Heinrich, M. C., and van de Rijn, M. (2004) The novel marker, DOG1, is expressed ubiquitously in gastrointestinal stromal tumors irrespective of KIT or PDGFRA mutation status. *Am. J. Pathol.* **165**, 107–113
3. Kashyap, M. K., Marimuthu, A., Kishore, C. J., Peri, S., Keerthikumar, S., Prasad, T. S., Mahmood, R., Rao, S., Ranganathan, P., Sanjeeviah, R. C., Vijayakumar, M., Kumar, K. V., Montgomery, E. A., Kumar, R. V., and Pandey, A. (2009) Genomewide mRNA profiling of esophageal squamous cell carcinoma for identification of cancer biomarkers. *Cancer Biol. Ther.* **8**, 36–46
4. Carles, A., Millon, R., Cromer, A., Ganguli, G., Lemaire, F., Young, J., Wasylyk, C., Muller, D., Schultz, I., Rabouel, Y., Dembélé, D., Zhao, C., Marchal, P., Ducray, C., Bracco, L., Abecassis, J., Poch, O., and Wasylyk, B. (2006) Head and neck squamous cell carcinoma transcriptome analysis by comprehensive validated differential display. *Oncogene* **25**, 1821–1831
5. Huang, X., Gollin, S. M., Raja, S., and Godfrey, T. E. (2002) High-resolution mapping of the 11q13 amplicon and identification of a gene, *TAOS1*, that is amplified and overexpressed in oral cancer cells. *Proc. Natl. Acad. Sci. U.S.A.* **99**, 11369–11374
6. Britschgi, A., Bill, A., Brinkhaus, H., Rothwell, C., Clay, I., Duss, S., Rebhan, M., Raman, P., Guy, C. T., Wetzel, K., George, E., Popa, M. O., Lilley, S., Choudhury, H., Gosling, M., Wang, L., Fitzgerald, S., Borawski, J., Baffoe, J., Labow, M., Gaither, L. A., and Bentires-Alj, M. (2013) Calcium-activated chloride channel ANO1 promotes breast cancer progression by activating EGFR and CAMK signaling. *Proc. Natl. Acad. Sci. U.S.A.* **110**, E1026–E1034
7. Shi, Z. Z., Shang, L., Jiang, Y. Y., Hao, J. J., Zhang, Y., Zhang, T. T., Lin, D. C., Liu, S. G., Wang, B. S., Gong, T., Zhan, Q. M., and Wang, M. R. (2013) Consistent and differential genetic aberrations between esophageal dysplasia and squamous cell carcinoma detected by array comparative genomic hybridization. *Clin. Cancer Res.* **19**, 5867–5878
8. Yang, Y. D., Cho, H., Koo, J. Y., Tak, M. H., Cho, Y., Shim, W. S., Park, S. P., Lee, J., Lee, B., Kim, B. M., Raouf, R., Shin, Y. K., and Oh, U. (2008) TMEM16A confers receptor-activated calcium-dependent chloride conductance. *Nature* **455**, 1210–1215
9. Schroeder, B. C., Cheng, T., Jan, Y. N., and Jan, L. Y. (2008) Expression cloning of TMEM16A as a calcium-activated chloride channel subunit. *Cell* **134**, 1019–1029
10. Caputo, A., Caci, E., Ferrera, L., Pedemonte, N., Barsanti, C., Sondo, E.,

- Pfeffer, U., Ravazzolo, R., Zegarra-Moran, O., and Galiotta, L. J. (2008) TMEM16A, a membrane protein associated with calcium-dependent chloride channel activity. *Science* **322**, 590–594
11. Huang, F., Wong, X., and Jan, L. Y. (2012) International Union of Basic and Clinical Pharmacology. LXXXV: calcium-activated chloride channels. *Pharmacol. Rev.* **64**, 1–15
 12. Cho, H., Yang, Y. D., Lee, J., Lee, B., Kim, T., Jang, Y., Back, S. K., Na, H. S., Harfe, B. D., Wang, F., Raouf, R., Wood, J. N., and Oh, U. (2012) The calcium-activated chloride channel anoctamin 1 acts as a heat sensor in nociceptive neurons. *Nat. Neurosci.* **15**, 1015–1021
 13. Zhang, C. H., Li, Y., Zhao, W., Lifshitz, L. M., Li, H., Harfe, B. D., Zhu, M. S., and ZhuGe, R. (2013) The TMEM16A Ca²⁺-activated Cl⁻ channel in airway smooth muscle contributes to airway hyperresponsiveness. *Am. J. Respir. Crit. Care Med.* **187**, 374–381
 14. Rock, J. R., Futtner, C. R., and Harfe, B. D. (2008) The transmembrane protein TMEM16A is required for normal development of the murine trachea. *Dev. Biol.* **321**, 141–149
 15. Duvvuri, U., Shiwerski, D. J., Xiao, D., Bertrand, C., Huang, X., Edinger, R. S., Rock, J. R., Harfe, B. D., Henson, B. J., Kunzelmann, K., Schreiber, R., Seethala, R. S., Egloff, A. M., Chen, X., Lui, V. W., Grandis, J. R., and Gollin, S. M. (2012) TMEM16A induces MAPK and contributes directly to tumorigenesis and cancer progression. *Cancer Res.* **72**, 3270–3281
 16. Perez-Cornejo, P., Gokhale, A., Duran, C., Cui, Y., Xiao, Q., Hartzell, H. C., and Faundez, V. (2012) Anoctamin 1 (Tmem16A) Ca²⁺-activated chloride channel stoichiometrically interacts with an ezrin-radixin-moesin network. *Proc. Natl. Acad. Sci. U.S.A.* **109**, 10376–10381
 17. De La Fuente, R., Namkung, W., Mills, A., and Verkman, A. S. (2008) Small-molecule screen identifies inhibitors of a human intestinal calcium-activated chloride channel. *Mol. Pharmacol.* **73**, 758–68
 18. Namkung, W., Phuan, P. W., and Verkman, A. S. (2011) TMEM16A inhibitors reveal TMEM16A as a minor component of calcium-activated chloride channel conductance in airway and intestinal epithelial cells. *J. Biol. Chem.* **286**, 2365–2374
 19. Kumar, S., Namkung, W., Verkman, A. S., and Sharma, P. K. (2012) Novel 5-substituted benzyloxy-2-arylbenzofuran-3-carboxylic acids as calcium activated chloride channel inhibitors. *Bioorg. Med. Chem.* **20**, 4237–4244
 20. Huang, F., Zhang, H., Wu, M., Yang, H., Kudo, M., Peters, C. J., Woodruff, P. G., Solberg, O. D., Donne, M. L., Huang, X., Sheppard, D., Fahy, J. V., Wolters, P. J., Hogan, B. L., Finkbeiner, W. E., Li, M., Jan, Y. N., Jan, L. Y., and Rock, J. R. (2012) Calcium-activated chloride channel TMEM16A modulates mucin secretion and airway smooth muscle contraction. *Proc. Natl. Acad. Sci. U.S.A.* **109**, 16354–16359
 21. Cheeseright, T., Mackey, M., Rose, S., and Vinter, A. (2006) Molecular field extrema as descriptors of biological activity: definition and validation. *J. Chem. Inf. Model.* **46**, 665–676
 22. Cheeseright, T. J., Mackey, M. D., Melville, J. L., and Vinter, J. G. (2008) FieldScreen: virtual screening using molecular fields. Application to the DUD data set. *J. Chem. Inf. Model.* **48**, 2108–17
 23. Duan, J., Dixon, S. L., Lowrie, J. F., and Sherman, W. (2010) Analysis and comparison of 2D fingerprints: insights into database screening performance using eight fingerprint methods. *J. Mol. Graph. Model.* **29**, 157–170
 24. Sastry, M., Lowrie, J. F., Dixon, S. L., and Sherman, W. (2010) Large-scale systematic analysis of 2D fingerprint methods and parameters to improve virtual screening enrichments. *J. Chem. Inf. Model.* **50**, 771–784
 25. Fallah, G., Romer, T., Detro-Dassen, S., Braam, U., Markwardt, F., and Schmalzing, G. (2011) TMEM16A(a)/anoctamin-1 shares a homodimeric architecture with CLC chloride channels. *Mol. Cell Proteomics* **10**, M110.004697
 26. Sheridan, J. T., Worthington, E. N., Yu, K., Gabriel, S. E., Hartzell, H. C., and Tarran, R. (2011) Characterization of the oligomeric structure of the Ca²⁺-activated Cl⁻ channel Ano1/TMEM16A. *J. Biol. Chem.* **286**, 1381–1388
 27. Bill, A., Schmitz, A., Albertoni, B., Song, J. N., Heukamp, L. C., Walrafen, D., Thorwirth, F., Verveer, P. J., Zimmer, S., Meffert, L., Schreiber, A., Chatterjee, S., Thomas, R. K., Ullrich, R. T., Lang, T., and Famulok, M. (2010) Cytohesins are cytoplasmic ErbB receptor activators. *Cell* **143**, 201–211
 28. Mathes, C., Friis, S., Finley, M., Liu, Y. (2009) QPatch: the missing link between HTS and ion channel drug discovery. *Comb. Chem. High Throughput Screen.* **12**, 78–95
 29. Tian, Y., Schreiber, R., and Kunzelmann, K. (2012) Anoctamins are a family of Ca²⁺ activated Cl⁻ channels. *J. Cell Sci.* **125**, 4991–4998
 30. Namkung, W., Thiagarajah, J. R., Phuan, P. W., and Verkman, A. S. (2010) Inhibition of Ca²⁺-activated Cl⁻ channels by gallotannins as a possible molecular basis for health benefits of red wine and green tea. *FASEB J.* **24**, 4178–4186
 31. Zhang, J., Li, L., Kim, S. H., Hagerman, A. E., and Lü, J. (2009) Anti-cancer, anti-diabetic and other pharmacologic and biological activities of pentagalloyl-glucose. *Pharm. Res.* **26**, 2066–2080
 32. Tien, J., Lee, H. Y., Minor, D. L., Jr., Jan, Y. N., and Jan, L. Y. (2013) Identification of a dimerization domain in the TMEM16A calcium-activated chloride channel (CaCC). *Proc. Natl. Acad. Sci. U.S.A.* **110**, 6352–6357
 33. Misumi, Y., Misumi, Y., Miki, K., Takatsuki, A., Tamura, G., and Ikehara, Y. (1986) Novel blockade by brefeldin A of intracellular transport of secretory proteins in cultured rat hepatocytes. *J. Biol. Chem.* **261**, 11398–11403
 34. Lippincott-Schwartz, J., Donaldson, J. G., Schweizer, A., Berger, E. G., Hauri, H. P., Yuan, L. C., and Klausner, R. D. (1990) Microtubule-dependent retrograde transport of proteins into the ER in the presence of brefeldin A suggests an ER recycling pathway. *Cell* **60**, 821–836
 35. Abriel, H., and Staub, O. (2005) Ubiquitylation of ion channels. *Physiology* **20**, 398–407
 36. Claessen, J. H., Kundrat, L., and Ploegh, H. L. (2012) Protein quality control in the ER: balancing the ubiquitin checkbook. *Trends Cell Biol.* **22**, 22–32
 37. Dalemans, W., Barbry, P., Champigny, G., Jallat, S., Dott, K., Dreyer, D., Crystal, R. G., Pavirani, A., Lecocq, J. P., and Lazdunski, M. (1991) Altered chloride ion channel kinetics associated with the Δ F508 cystic fibrosis mutation. *Nature* **354**, 526–528
 38. Ward, C. L., Omura, S., and Kopito, R. R. (1995) Degradation of CFTR by the ubiquitin-proteasome pathway. *Cell* **83**, 121–127
 39. Tian, Y., Schreiber, R., Wanitchakool, P., Kongsuphol, P., Sousa, M., Uliyakina, I., Palma, M., Faria, D., Traynor-Kaplan, A. E., Fragata, J. I., Amaral, M. D., and Kunzelmann, K. (2013) Control of TMEM16A by INO-4995 and other inositolphosphates. *Br. J. Pharmacol.* **168**, 253–265
 40. Lins, L., and Brasseur, R. (1995) The hydrophobic effect in protein folding. *FASEB J.* **9**, 535–540
 41. Neklesa, T. K., Tae, H. S., Schneekloth, A. R., Stulberg, M. J., Corson, T. W., Sundberg, T. B., Raina, K., Holley, S. A., and Crews, C. M. (2011) Small-molecule hydrophobic tagging-induced degradation of HaloTag fusion proteins. *Nat. Chem. Biol.* **7**, 538–543
 42. Mazzone, A., Eisenman, S. T., Strega, P. R., Yao, Z., Ordog, T., Gibbons, S. J., and Farrugia, G. (2012) Inhibition of cell proliferation by a selective inhibitor of the Ca²⁺-activated Cl⁻ channel, Ano1. *Biochem. Biophys. Res. Commun.* **427**, 248–253
 43. Jin, X., Shah, S., Liu, Y., Zhang, H., Lees, M., Fu, Z., Lippiat, J. D., Beech, D. J., Sivaprasadarao, A., Baldwin, S. A., Zhang, H., and Gamper, N. (2013) Activation of the Cl⁻ channel ANO1 by localized calcium signals in nociceptive sensory neurons requires coupling with the IP₃ receptor. *Sci. Signal.* **6**, ra73